Two-color Counter-countermeasure for the Crossed Array Tracker

S. H. Lee*, J. S. Oh*, K.S. Doo*, D. S. Seo**, and J. S. Choi*
Department of Image Engineering, Graduate School of Advanced Imaging Science, Multimedia and Film, Chung-Ang University, 221 Huksuk-Dong, Dongjak-Ku, Seoul, Korea
**Dept. of Electronic Eng., Myoung-Ji University, 449-728, Yongin, Kyonggido, Korea
Tel.: +82-2-820-5295, FAX: +82-2-814-5404
E-mail: sukhan@candy.ee.cau.ac.kr

Abstract: Infrared (IR) seeker identifies the location of a target by detecting the infrared energy radiated from the target, and enables the missile to track the target. To improve the tracking performance, a counter-countermeasure (CCM) is essential to minimize the effect of the countermeasure (CM), which is operated by a target to protect itself. In this paper, we propose a crossed array tracker (CAT) using two-color CCM algorithm. The CAT using the proposed algorithm shows better tracking performance by minimizing the effect of CM.

1. Introduction

IR seeker, which is mounted on a homing missile, identifies the location of a target by detecting the infrared energy radiated from the target, and enables the missile to track the target. A target operates a CM such as flares to protect itself from a homing missile. To improve the tracking performance, a CCM is essential to minimize the effect of the countermeasure [1], [2]. In this paper, we propose a CAT using the two-color CCM algorithm. The proposed algorithm uses two detection bands; one is for the target detection and the other is for the flare detection. The proposed algorithm calculates the ratio between these two bands to extract only target signals. To estimate the tracking performance of the CAT, we analyze the result under the ideal condition without flares and noise and compare it with those of various dynamic conditions for a target and flares. In the case that a target and flares are in the field of view (FOV) of CAT simultaneously, the CAT using the proposed algorithm shows better tracking performance by minimizing the effect of the CM.

This paper is organized as follows. In Section 2, the fundamental characteristics of CAT are described, and the proposed CCM algorithm is presented in Section 3. In Section 4, the simulation blocks are descripted, and the simulation results are analyzed in Section 5. Finally a brief conclusion is given in Section 6.

2. The characteristics of Crossed Array Tracker

CAT is composed of four independent IR sensors, and located behind a optical system. Fig.1 shows the crossed array detector and its outputs. The optics move the target image along the nutation circle centered at the real position of the target in its FOV. The target image produces pulse signals as it passes by each detector. In the absence of the error, the center of the nutation circle coincides with that of the detector array and the detector array produces pulses at constant timing intervals. With the error, the center of the nutation circle doesn't coincide with that of the detector array and the timing interval is no longer constant. Using the position of the produced pulses and reference timing, the position of the target in FOV can be estimated. The distance between the center of the nutation circle and that of the detector array means the tracking error [3], [4], [5].

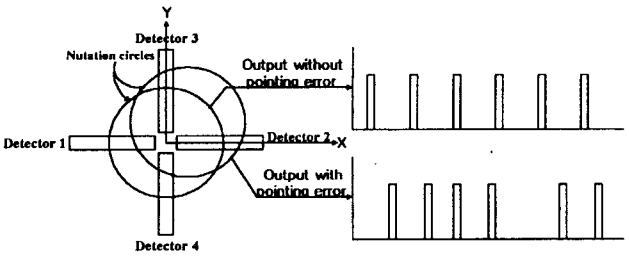

Fig.1 Crossed array detector and its output pulses

In Fig.2, the center of the nutation circle is the tracking error and it is expressed as Eq.(1) and Eq.(2), which are the equations of the center of the nutation circle R_N and the phase ϕ. The phase ϕ generates the timing interval of the output signal of the detector.

$$x(t) = R_N \times \cos(\phi(t)/2) \quad (1)$$

$$y(t) = R_N \times \cos(\pi + \phi(t)/2) \quad (2)$$

Fig.3 shows the tracking area of CAT. The length of the detector is R_D, and the slashed area is the linear tracking field. Each of the vertical length and the horizontal length of the field is equal to the diameter of the nutation circle. The distance between the center of the nutation circle and that of the detector should be smaller then R_N so that the linear target tracking is enabled [4], [5]. The detector used in our paper has the length of 152 pixels and the width of 18 pixels.

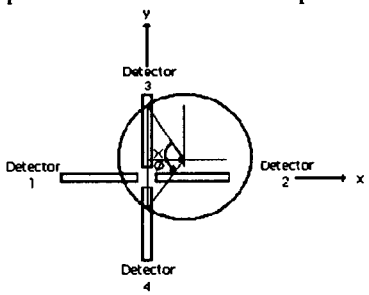

Fig.2 Target image nutation circles.

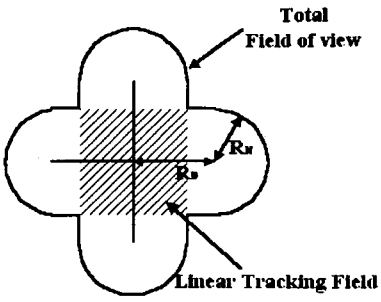

Fig.3 Crossed array tracking field.

3. Proposed CCM algorithm

The detection bands for a target and a flare are determined considering the radiation characteristics and the atmospheric transmission characteristics. Since the temperatures of a target and a flare are assumed to be 700K and 2000K, respectively, we use mid band (3 ~ 5 μ m) for a target detection and near band (1.5 ~ 1.7μ m) for a flare detection [1], [4], [7].

The temperature of a flare is much higher than that of a target. The flare radiates intensive energy in both bands, while the target radiates intensive energy only in mid band. Therefore, the ratio of a target signal between two bands is larger than that of a flare signal. From the histogram of this ratio, we get the ratio of the flare, which enables to discriminate the target signal from the flare signal, and the location of the target can be extracted [1], [2], [6].

The input signal of mid band and that of near band can be described as Eq.(3).

$$V_M = \sum_{i=1}^{I} V_{FMi} + V_{TM}, \quad V_N = \sum_{i=1}^{I} V_{FNi} + V_{TN}, \tag{3}$$

where, V_M and V_N are the input signal of mid band, and the input signal of near band respectively, and i means the number of flares.

The signal ratios of the input signals can be considered as following three cases.

Case 1. Only flares exist.

$$r_{MN,F} = \frac{\sum_{i=1}^{I} V_{FMi}}{\sum_{i=1}^{I} V_{FNi}}, \tag{4}$$

Case 2. One target and flares exist.

$$r_{MN,T+F} = \frac{\sum_{i=1}^{I} V_{FMi} + V_{TM}}{\sum_{i=1}^{I} V_{FNi} + V_{TN}}, \tag{5}$$

Case 3. Only one target exists.

$$r_{MN,T} = \frac{V_{TM}}{V_{TN}}, \tag{6}$$

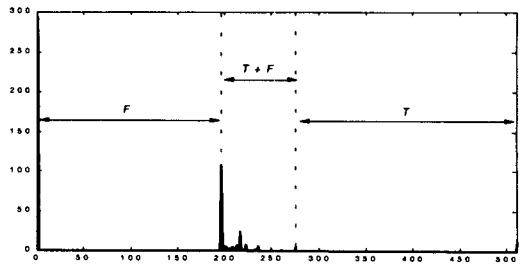

Fig.4 The histogram of the ratio of the two input signals.

here, V_N is very small, and the relationship among Eq.(4) ~ Eq.(6) is as follow.

$$r_{MN,F} < r_{MN,T+F} < r_{MN,T} \tag{7}$$

Fig.4 shows the histogram of the ratio of the input signals. In Fig.4, F, T+F, and T are produced by $r_{MN,F}$, $r_{MN,F+T}$, and $r_{MN,T}$ respectively. Moreover, the peak between F and T+F means $r_{MN,F}$. Therefore, if we choose $r_{MN,F}$ to be the threshold level of the ratio of the two input signals, only target signals can be extracted, and the final output Vo is given as Eq. (8).

$$V_O = r_{MN,T} + r_{MN,T+F} \tag{8}$$

4. Simulator of two-color CAT with proposed CCM

Fig.5 shows the simulation blocks. Inputs are given as the position errors and the radiation intensities of a target and flares. The final block outputs the location of the target obtained through the CCM block.

The IR crossed array detector block generates target signal and flare signal. The sampling time is 0.01 seconds, and 512 samples are generated. The noise generator block adds noise to the input signal to estimate the effects of various noise levels. The AGC block compensates the variation of the input signal for the next block. The CCM block extracts only target signals, and peak detector block detects the positions of pulses. The location of a target in FOV is computed in error calculator block. Finally, using the output of the error calculator, the tracking is performed by the tracking loop, which has type-I characteristic.

Fig.6(a) shows the output of the detector, and Fig.6(b) is the histogram of the ratio of the two input signals. Fig.6(c) shows the extraction of the position of the pulses of the target signal, and Fig.6(d) is the extracted positions of the target signal.

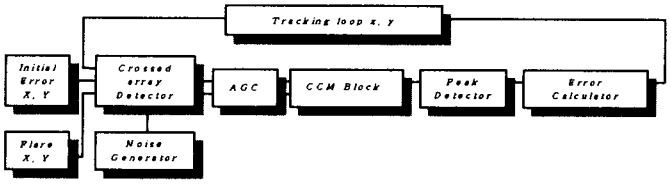

Fig.5 The simulation blocks

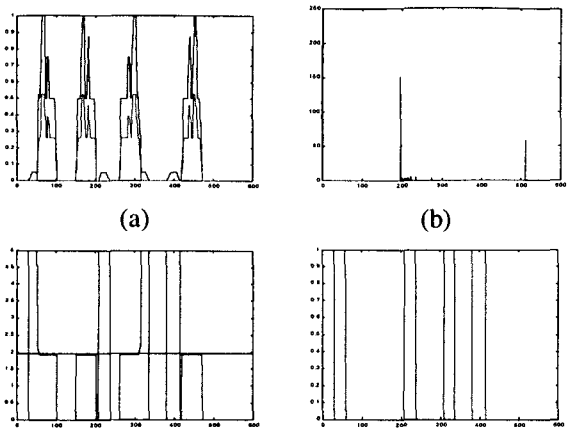

(a) (b)

(c) (d)

Fig.6 (a) The output of the detector block, (b) The histogram of the ratio of the signals, (c) The position of the target signal extraction, (d) The extracted position of the target signal.

5. Simulation results

The simulations are performed using MATLAB. The length of a detector is 152 pixels and the width of the detector is 18 pixels. The radius of the target and the flares are assumed to be 9, and 4.5 pixels respectively.

5.1 Tracking performances in ideal condition.

Fig.7 shows the tracking performances without noise, and with 10dB noise, respectively. The target is stationary and its initial error is (38, 38). With no noise, the tracking error converges absolutely to 0. With 10 dB noise the tracking error converges to almost 0. Fig.8 depicts the tracking performances for a moving target with constant speed. The initial errors are (38, 38), and (-40, 35) respectively. Since we use type-I tracking loop, the seeker tracks the target with a constant steady-state error. Table 1 shows the rms errors for various SNRs and initial errors.

5.2 Tracking performances for dynamic conditions with 3 flares.

The radiation characteristic and the trajectory of three flares are shown in Fig.9. The target ejects flares at 0.5 seconds, and the flares radiate their maximum energy at 1 second after the ejection and no energy after 3.5 seconds. Fig.10 shows the tracking performance of moving target with constant speed and 3 moving flares. The initial tracking errors are (40, 36), and (-32, 43), respectively, and 10dB noise is included. Fig.11 shows the tracking performance of CAT without CCM. The seeker using proposed CCM shows better tracking performances, since the seeker using CCM can remove the effect of the flares, and extracts precise target positions. Table 2 shows the averages of rms errors of CAT using proposed CCM, and CAT without CCM. Fig.12 presents the trajectories of the target and three flares. In the figure, 'O' marker means the movement of the target, and '+' marker means the trajectory of three flares. It also shows better performances of the seeker using proposed CCM.

6. Conclusion

In this paper, we proposed two-color CCM and performed simulations of various dynamic conditions. To minimize the effect of CM, we used mid band (3 ~ 5μ m) for target detection and near band (1.5 ~ 1.7μ m) for flare detection. And we verified that when one target and flares are in the field of view (FOV) of CAT simultaneously, the CAT using the proposed algorithm showed better tracking performance by minimizing the effect of CM.

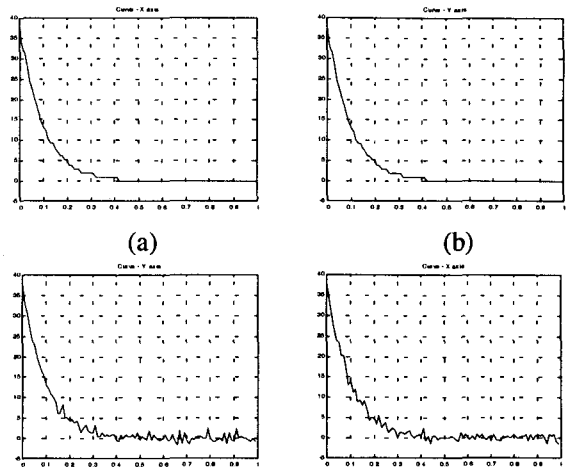

(a) (b)

(c) (d)

Fig.7 The tracking performance for a stationary target: (a) x-axis error without noise, (b) y-axis error without noise, (c) x-axis error with 10dB noise, (d) y-axis error with 10dB noise.

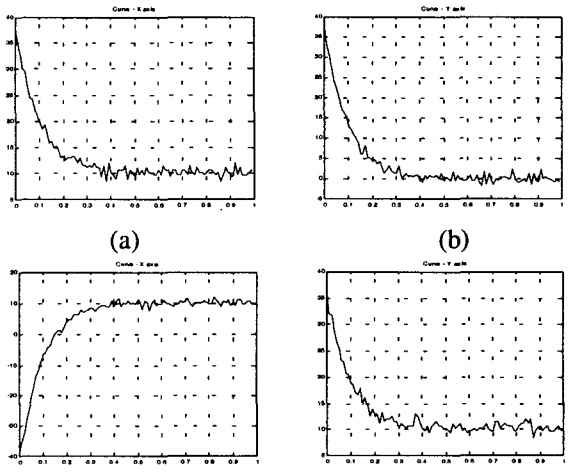

(a) (b)

(c) (d)

Fig.8 The tracking performance for a moving target with constant speed: (a) x-axis error, the initial tracking error is x = 38, (b) y-axis error, the initial tracking error is y = 38, (c) x-axis error, the initial tracking error is x = -40 , (d) y-axis error, the initial tracking error is y = 35.

Table 1: The rms errors for various SNR and initial errors.

SNR	Initial error X=45, Y = 30		Initial error X = -30, Y = 45	
	rms error		rms error	
	X	Y	X	Y
10dB	0.0778	0.0782	0.0655	0.0786
20dB	0.0703	0.0629	0.0616	0.0514
30dB	0.0357	0.0257	0.0369	0.0249

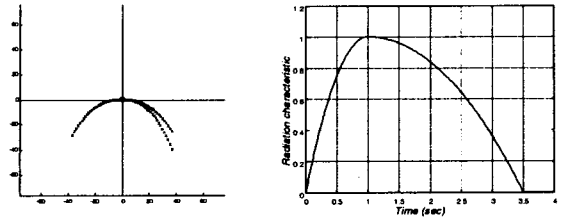

(a) (b)

Fig.9 (a) The trajectory of three flares in FOV, (b) The radiation characteristic of the flare.

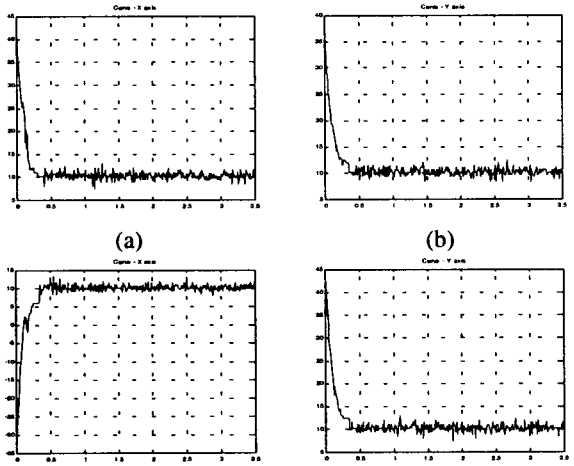

(a) (b)

(c) (d)

Fig.10 The tracking performance for a moving target when three flares and 10dB noise exist: (a) x-axis error, the initial tracking error is x = 40, (b) y-axis error, the initial tracking error is y = 36, (c) x-axis error, the initial tracking error is x = -32 , (d) y-axis error, the initial tracking error is y = 43.

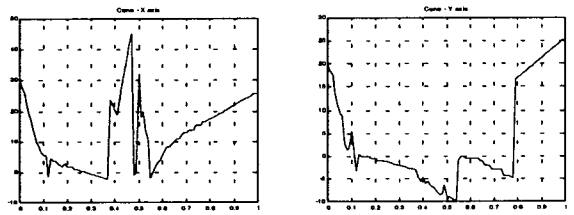

(a) (b)

Fig.11 The tracking performances of CAT without CCM: (a) x-axis error, (b) y-axis error.

Table 2: the average of rms errors of CAT using proposed CCM, and CAT without CCM.

Without CCM		With CCM	
rms error		rms error	
X	Y	X	Y
8.0357	6.8287	0.0969	0.1027

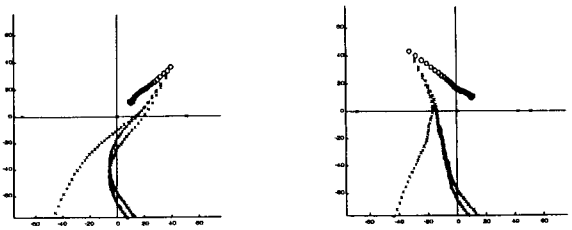

(a) (b)

Fig.12 The trajectories of the target and three flares in FOV: (a) The initial error is (40, 36), (b) The initial error is (-32, 43).

7. Acknowledgement

This work is supported by Automatic Control Research Center, Seoul National University, Seoul, Korea, and by the Ministry of Education, Seoul, Korea, under BK21 project. The authors would like to thank Dr. Inn-Eark Yoo in Agency Defense Development, Taejon, Korea, for helpful discussions.

References

[1] J.S.Oh, K.S.Doo, S.G.Jahng, D.S.Seo, J.S.Choi, "Acquisition Modeling of an Airborne Target", *Proc. ITC-CSCC '99, Niigata, Japan, Vol.1, pp106-109, July, 1999.*

[2] Ronald G. Driggers, Paul Cox, Timothy Edwards, *Introduction to Infrared and Electro Optical Systems,* Artech House, Boston, 1999.

[3] Richard D. Hudson JR, *Infrared System Engineering,* John Wiley & Sons Inc, New York, 1996.

[4] William L. Wolfe, George J. Zissis, *The Infrared Handbook,* Environmental Research Institute of Michigan, pp22.56-22.60, 1985.

[5] K.J.Choi, K.S.Doo, H.K.Hong, S.K.Jahng, J.S.Oh, D.S.Seo, J.S.Choi, "A Study on Analysis of Crossed Array Tracker and an Efficient Counter-countermeasure Algorithm", *Proc., KSPC, Seoul, Korea, Vol.11, pp723-726, October, 1998.*

[6] Frederick G. Smith, The Infrared & Electro-optical systems handbook Vol. 4, *Atmospheric Propagation of Radiation,* SPIE press, 1993.

[7] George J. Zisis, The Infrared & Electro-optical systems handbook Vol.1, *Sources of Radiation,* SPIE press, 1993.